Appl. Comput. Harmon. Anal. 29 (2010) 88–96

Contents lists available at ScienceDirect

Applied and Computational Harmonic Analysis

www.elsevier.com/locate/acha

Case Study

Analysis of transient multiexponential signals using cepstral deconvolution

Abdussamad U. Jibia *, Momoh-Jimoh E. Salami, Othman O. Khalifa, A.M. Aibinu

Kulliyyah of Engineering, International Islamic University Malaysia, Jalan Gombak, 50728, Kuala Lumpur, Malaysia

ARTICLE INFO

Article history:
Received 27 May 2009
Accepted 12 June 2009
Available online 17 June 2009
Communicated by Charles K. Chui

Keywords:
Multiexponential
Homomorphic deconvolution
Cepstrum
Lifter
Fluorescence

ABSTRACT

We propose and test a new method of multiexponential transient signal analysis. The method based on cepstral deconvolution is fast and computationally inexpensive. The multiexponential signal is initially converted to a deconvolution model using Gardners' transformation after which the proposed method is used to deconvolve the data. Simulation and experimental results indicate that this method is good for determining the number of components but performs poorly in accurately estimating the decay rates. Influence of noise is not considered in this paper.

1. Introduction

There is enough motivation in science and technology for the study of multicomponent transients of the form

$$S(\tau) = \sum_{i=1}^{M} A_i \exp(-\lambda_i \tau) \tag{1}$$

where $0 < \tau < \infty$, M is the number of components, A_i is the amplitude of the ith component, and λ_i the corresponding decay rate. For example, the fluorescence decay of most biological macromolecules is more complex than a single exponential, the emission process in deep-level transient spectroscopy is described by exponentials with time constants depending on the temperature and energy of the traps in the band gap. The number of trap levels determines the number of exponentials M.

A major problem emphasized by all researchers on multiexponential signal analysis is the fact that these signals do not form an orthogonal base. As early as 1795, Prony [1] proposed a method that could decompose a small number of exponentials with similar amplitudes but different time constants. Much later, Lanczos [2] demonstrated that three exponential curves with similar time constants could be fitted accurately with two exponential models with significantly different amplitudes and time constants. He further showed that residual plots for double and triple exponential fits look very similar but are not helpful in deciding which fit is better. This, he showed, was a consequence of nonorthogonality of the exponentials. Another problem associated with the analysis of multiexponential signals is their fundamental ill-posedness. This means small perturbations in the input signal can yield unrealistically high perturbations in the decomposition results.

* Corresponding author.
E-mail address: aujibia@gmail.com (A.U. Jibia).

1063-5203/$ – see front matter
doi:10.1016/j.acha.2009.06.002

Prony's method was followed by a number of attempts to find real components from experimental data. In a pioneer paper, Gardner et al. [3] proposed a model in which a nonlinear change of variables is used to convert the original signal into a convolution integral which could be deconvolved by Fourier Transform technique. The difficulty at that time was the non-availability of effective algorithms for the computation of Fourier integrals. This problem was solved later by Schlesinger [4] using the fast Fourier transform (FFT). Nichols et al. [5] further modified the Gardners' transformation by introducing a weighting factor, α, in the nonlinear transformation.

In [6], Salami and Sidek used the modified Gardners' transformation to convert the signal in (1) into a discrete convolution model whose input is a train of weighted delta functions containing the parameters to be determined. This successfully removed the nonorthogonality problem associated with the original signal. Deconvolution was done using a single parameter deconvolution model. SVD-ARMA parametric method was then used to process the deconvolved data.

In this paper, homomorphic deconvolution technique is used to deconvolve the model resulting from the application of modified Gardners' transformation. Its advantages include computational simplicity, speed and elimination of the data length constraint encountered in [6]. In addition to these, it does not require additional modeling as in previous approaches. Furthermore, unlike the least squares method for example, our approach does not require an a priori knowledge of the number of components. Another novelty in this paper is a new procedure for the determination of sampling conditions.

2. Signal preparation

This stage consisting of modified Gardners' transformation, and sampling is meant to solve the problem of nonorthogonality associated with multicomponent exponential signal and to prepare the signal for the application of homomorphic deconvolution technique.

2.1. Development of a convolution model

Eq. (1) can be expressed as

$$S(\tau) = \int_0^\infty g(\lambda) \exp(-\lambda\tau)\, d\lambda \tag{2}$$

This integral belongs to the more general class of Fredholm integral of the first kind which are known to be ill-posed. In this special case of multiexponential signals the spectral distribution function $g(\lambda)$ is given by

$$g(\lambda) = \sum_{i=1}^{M} A_i \delta(\lambda - \lambda_i) \tag{3}$$

and contains all the parameters of interest. Multiplying both sides of (2) by τ^α ($\alpha > 0$) and applying the Gardners' transformation [3], $\tau = e^t$ and $\lambda = e^{-r}$ results in the convolution integral

$$y(t) = \int_{-\infty}^{\infty} x(\lambda) h(t - \lambda)\, d\lambda \tag{4}$$

where

$$y(t) = \exp(\alpha t) S\big(\exp(t)\big) \tag{5a}$$

$$x(t) = \exp\big((\alpha - 1)t\big) g\big(e^{-t}\big) \tag{5b}$$

$$h(t) = \exp(\alpha t) \exp\big(-e^t\big) \tag{5c}$$

This is now a standard deconvolution problem in which $x(t)$ is the unknown input consisting of a series of weighted delta functions, $h(t)$ is the impulse response and $y(t)$ is the output observation.

It can be shown [7] that the unknown input distribution function is given by

$$x(t) = \sum_{i=1}^{M} B_i \delta(t + \ln \lambda_i) \tag{6}$$

where $B_i = A_i(\lambda_i)^{-\alpha}$.

2.2. Selecting the sampling conditions

Eq. (4) is now converted into a discrete-time deconvolution problem. This is achieved by considering $y(t)$ to be the output of a linear, time-invariant system which has the impulse response $h(t)$ and an input $x(t)$. With this consideration, $y(t)$ is uniformly sampled at the rate of $f_s = \frac{1}{\Delta t}$, where Δt is the sampling interval. The sampling rate depends on the bandwidth of the basic pulse while the number of samples required depends on the data.

The exponential function $e^{-\lambda\tau}$, $0 \leqslant \tau \leqslant \infty$ maps to the system function $h(t) = \exp(\alpha t)\exp[-\exp(t)]$, $-\infty \leqslant t \leqslant \infty$.

If we let $t = n\Delta t$ in the convolution integral of Eq. (4) we obtain

$$y(n\Delta t) \approx \Delta t \sum_{-\infty}^{\infty} x(m\Delta t) h\big((n-m)\Delta t\big) \tag{7}$$

Sampling at the rate of $\frac{1}{\Delta t}$ and letting $y[n] = y(n\Delta t)$, $x[n] = x(n\Delta t)$ and $h[n] = \Delta t(h(n\Delta t))$ simplifies this expression to

$$y[n] = \sum_{-\infty}^{\infty} x[m]h[n-m] \tag{8}$$

The bandwidth of the conceptual system can be determined using the concept of noise equivalent bandwidth (NEB). The NEB is the bandwidth of an ideal bandpass filter that would pass the same amount of white noise power as the system being analyzed. The NEB and the 3-dB bandwidth are sometimes used interchangeably, particularly when the detailed information about the system response is not available [8]. The NEB of a system with impulse response $h(t)$ is given by [9]

$$B = \frac{\int_{-\infty}^{\infty} |h(t)|^2\, dt}{2[\int_{-\infty}^{\infty} h(t)\, dt]^2} \tag{9}$$

Now let

$$M = \int_{-\infty}^{\infty} h(t)\, dt = \int_{-\infty}^{\infty} e^{\alpha t} e^{-e^t}\, dt \tag{10}$$

Integration yields

$$M = \left[\frac{e^{\alpha t}\exp(-e^t)}{2\alpha}\right]_{-\infty}^{\infty} \tag{11}$$

and let

$$N = \int_{-\infty}^{\infty} \big|h(t)\big|^2\, dt = \int_{-\infty}^{\infty} \big|e^{\alpha t} e^{-e^t}\big|^2\, dt = \int_{-\infty}^{\infty} e^{2\alpha t} e^{-2e^t}\, dt \tag{12}$$

Again, integration yields

$$N = \left[\frac{e^{2\alpha t} e^{-2e^t}}{4\alpha}\right]_{-\infty}^{\infty} \tag{13}$$

But from (9)

$$B = \frac{[\frac{e^{2\alpha t} e^{-2e^t}}{4\alpha}]_{-\infty}^{\infty}}{2\{[\frac{e^{\alpha t}\exp(-e^t)}{2\alpha}]_{-\infty}^{\infty}\}^2} \tag{14}$$

In practice, the range of t will be finite. Let the lower and upper limit be T_1 and T_2 respectively. Then,

$$B = \frac{\frac{1}{4\alpha}\{e^{2(\alpha T_2 - e^{T_2})} - e^{2(\alpha T_1 - e^{T_1})}\}}{\frac{1}{2\alpha^2}\{e^{(\alpha T_2 - e^{T_2})} - e^{(\alpha T_1 - e^{T_1})}\}^2} \tag{15}$$

The graph of $h(t)$ against time is shown in Fig. 1 for different values of α. From the plot, it is sufficient to select $T_2 = 0$ and $T_1 = -T_{min}$ (where $-T_{min}$ is some arbitrary minimum value of t). Eq. (15) then reduces to:

$$B = \frac{\frac{\alpha}{2}[0.135 - e^{2(\alpha T_{min} - e^{T_{min}})}]}{[0.8734 - e^{(\alpha T_{min} - e^{T_{min}})}]^2} \tag{16}$$

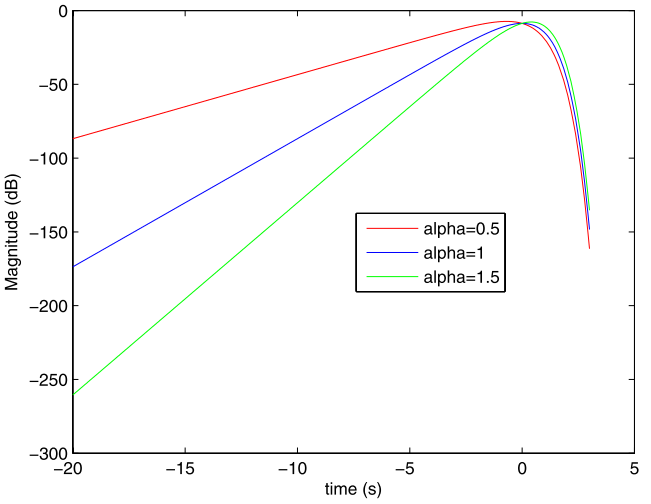

Fig. 1. Graph of $h(t)$ against time.

When T_{min} is sufficiently large (say, $\geqslant 5$ s) and $\alpha \geqslant 0.5$, the exponential terms become negligibly small and we have

$$B = \frac{\alpha}{2} \tag{17}$$

Thus, for unaliased sampling of $y(t)$, the sampling frequency, f_s, must satisfy

$$f_s \geqslant 2B = \alpha \tag{18}$$

In practice, the range of m in Eq. (8) must be finite which suggests that both $y[n]$ and $h[n]$ will have to be truncated. Choosing the upper and lower data cut-off points to be n_{max} and n_{min} respectively, we can rewrite Eq. (8) as

$$y[n] = \sum_{m=-n\,min}^{n_{max}} x[m]h[n-m] \tag{19}$$

where $N = n_{max} - n_{min} + 1$ and the sampling interval is $\Delta t \leqslant \frac{1}{\alpha}$.

3. Homomorphic deconvolution

At the first glance, one would be tempted to use the commonest approach to deconvolution, the inverse filtering to extract $x[n]$ from the discrete convolution model of (19). In the inverse filtering, unwanted components of a convolution are removed by filtering with a linear system whose system function is the reciprocal of the Fourier transform of these components. Straightforward as it may sound, this approach has a number of drawbacks. First, it is only reasonable for those situations in which we have a detailed model or description of the components to be removed. Secondly, the inverse filtering approach enhances noise and a number of attempts continue to emerge to solve the problem of noise enhancement. Thirdly, application of inverse filtering more easily done in the frequency domain, would convert the problem into a spectral analysis one requiring additional modeling using conventional spectrum estimation techniques. To avoid the computational problems of inverse filtering we propose homomorphic deconvolution technique which is based on the notion of generalized inverse filtering proposed by Oppenheim and Schafer [10]. A number of reasons make homomorphic deconvolution technique suitable for this analysis. First, it will eliminate the data length constraint associated with inverse filtering (see [6]). Secondly, it has the ability to detect periodic structures in logarithmic spectrum and this can be used to detect the exponential constants given in (6). In addition, it requires less complex computation than inverse filtering since it can be implemented using the FFT algorithm. This points to its fourth advantage-speed.

The canonic representation for homomorphic deconvolution (also called cepstral deconvolution) system for the separation of two convolved functions, say, $x[n]$ and $h[n]$ is shown in Fig. 2. For a detailed description of this method the reader is referred to [10–12]. The main difficulty of this method is the choice of the linear lifter that will separate $\hat{h}[n]$ and $\hat{x}[n]$ in the quefrency domain. This is complicated by the nonlinearity of the complex cepstrum which implies that a slight modification of the input signal might lead to the reconstructed signal being completely different from the input. An additional problem is the fact that there is no clear demarcation in the regions of support for $x[n]$ and $h[n]$ in the original convolution model. With these considerations we proceed as follows.

Depending on whether the logarithm used is real or complex, the output of the first IDTFT is called real cepstrum (or simply the cepstrum) or complex cepstrum. Eqs. (20) and (21) give the complex cepstrum and the cepstrum respectively.

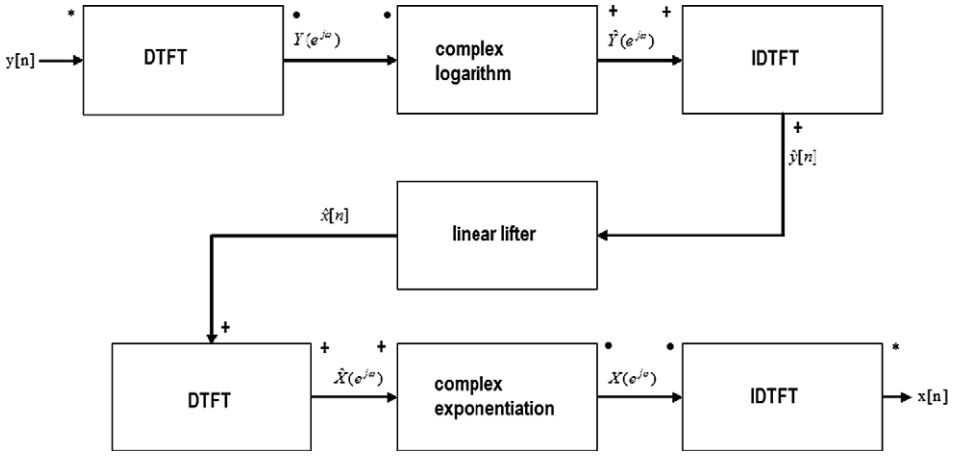

Fig. 2. Canonic representation of homomorphic deconvolution system.

$$\hat{y}[n] = \frac{1}{2\pi}\int_{-\pi}^{\pi} \log\big[Y(e^{j\omega})\big]e^{j\omega n}\,d\omega$$
$$= \frac{1}{2\pi}\int_{-\pi}^{\pi} \big[\log\big|Y\big(e^{j\omega}\big)\big| + j\arg\big(Y\big(e^{j\omega}\big)\big)\big]e^{j\omega n}\,d\omega \tag{20}$$

$$c_y[n] = \frac{1}{2\pi}\int_{-\pi}^{\pi} \log\big|Y\big(e^{j\omega}\big)\big|e^{j\omega n}\,d\omega \tag{21}$$

While it is easier to compute the cepstrum, it has the disadvantage of not being invertible. This is because unlike the complex cepstrum it does not retain phase information.

One of the important properties of the complex cepstrum is that it is causal when the input sequence $y[n]$ is minimum phase [10]. We can use this property to find an expression for the complex cepstrum in terms of the real cepstrum. To do that, the input signal must be converted to a minimum phase one. This is easily achieved by applying the concept of exponential weighting [13]. This involves the multiplication of the input sequence by a real number ξ^n:

$$y'[n] = \xi^n y[n] \quad 0 < \xi < 1 \tag{22}$$

Relationship between the cepstrum and complex cepstrum can be obtained by noting that, if $y[n]$ is real, then $\log|Y(e^{j\omega})|$ is real and even function of ω. This implies that,

$$c'_y[n] = \frac{\hat{y}'[n] + \hat{y}'[-n]}{2} \tag{23}$$

In other words, the cepstrum is the even part of the complex cepstrum.

The complex cepstrum can thus be expressed as:

$$\hat{y}'[n] = c'_y[n]u_+[n] \tag{24}$$

where

$$u_+(n) = \begin{cases} 1 & n = 0 \\ 2 & n > 0 \\ 0 & n < 0 \end{cases} \tag{25}$$

When the DFT is used, the cepstrum is time-aliased and given by

$$c'_p[n] = \sum_{k=-\infty}^{\infty} c'_y(n + kN) \tag{26}$$

To compute the complex cepstrum we can then write:

$$\hat{y}'[n] = \begin{cases} c'_p[n] & n = 0 \\ 2c'_p[n] & 1 \leqslant n \leqslant N_0 \\ 0 & N_0 + 1 \leqslant n \leqslant N - 1 \end{cases} \tag{27}$$

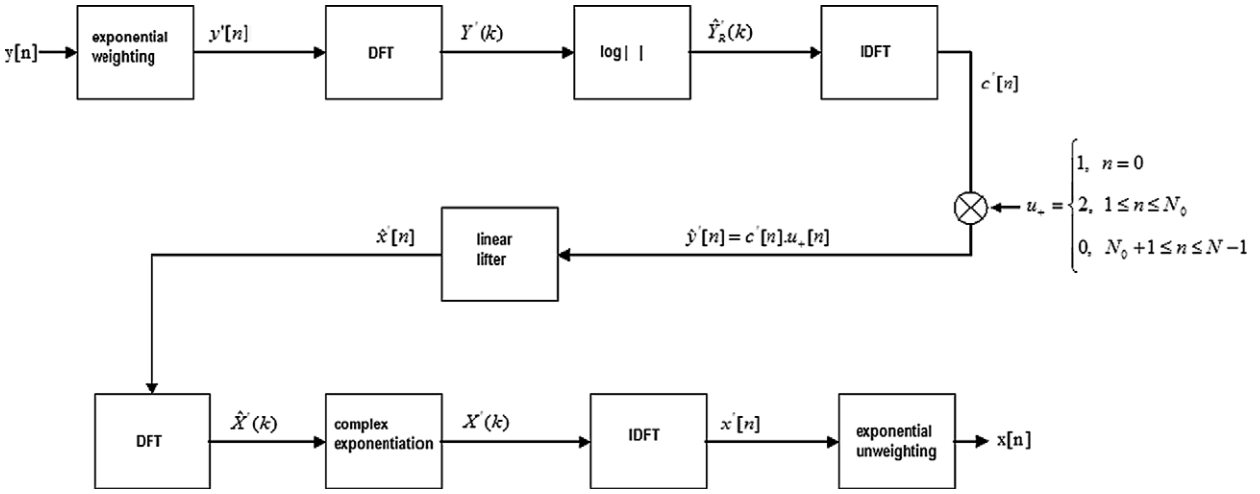

Fig. 3. Block diagram for the analysis of multiexponential signals using homomorphic deconvolution.

N_0 is the cepstrum cut-off point which must be carefully selected to get good results. The choice of N_0 is critical to the performance of this method.

Next, homomorphic filtering is achieved by forming a modified complex cepstrum

$$\hat{y}'_l = l[n]\hat{y}'[n] \tag{28}$$

where $l[n]$ is a window (or lifter) which selects a portion of the complex cepstrum for inverse processing. This is achieved as follows:

For $n \geqslant 1$

$$q(1) = \hat{y}'(1) \tag{29a}$$

$$q(n) = \gamma\,\hat{y}'[n] + (1-\gamma)q(n-1) \tag{29b}$$

and for $n \leqslant N_0$

$$w(N_0) = \hat{y}'(N_0) \tag{30a}$$

$$w(n) = \gamma\,\hat{y}'[n] + (1-\gamma)w(n+1) \tag{30b}$$

so that the output variable would be

$$\hat{y}'_l(n) = 0.5\big(q(n) + w(n)\big) \tag{31}$$

γ is the variable filter coefficient such that $0 \leqslant \gamma \leqslant 1$.

Taking the forward DFT of $\hat{y}'_l(n)$ followed by exponentiation, inverse DFT and exponential unweighting yields $x[n]$ with dominant peaks at $\ln\lambda_i$, $i = 1, 2, \ldots, M$.

In sum, the procedure we have proposed here for extracting the signal $x[n]$ from the discrete convolution model of (19) consists of the following steps:

- Convert the input signal $y[n]$ to minimum phase by exponential weighting.
- Compute the cepstrum.
- Convert the real cepstrum to complex cepstrum.
- Apply the appropriate cepstral lifter.
- Compute the inverse complex cepstrum.
- Perform exponential unweighting.

The complete flow diagram for the procedure is shown in Fig. 3.

4. Simulation results

The method outlined above was coded and tested in a MATLAB® environment using the following synthetically generated monoexponential and biexponential signals:

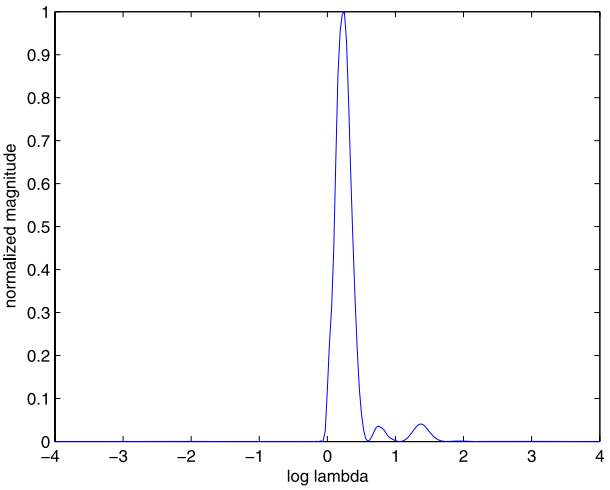

Fig. 4. Graph of distribution function for $S_1(\tau)$ from simulation.

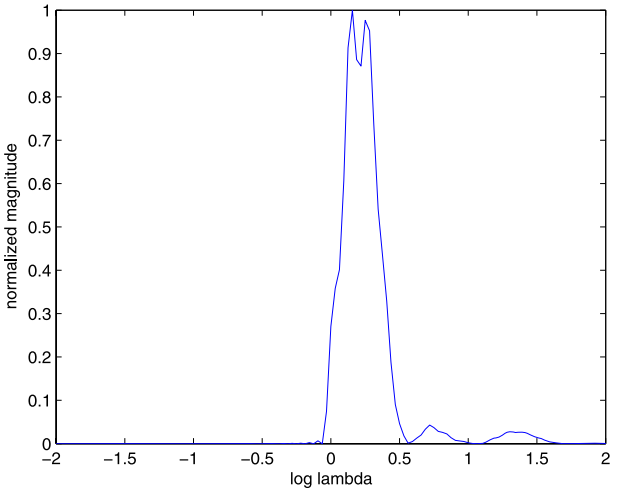

Fig. 5. Graph of distribution function for $S_2(\tau)$ from simulation.

Table 1
Percentage differences between the expected and estimated decay rates for $S_1(\tau)$ and $S_2(\tau)$.

Signal	i	Estimated log of decay rate ($\ln\hat{\lambda}_i$)	Estimated decay rate ($\hat{\lambda}_i$)	Expected value of decay rate (λ_i)	Expected value of log of decay rate ($\ln\lambda_i$)	Percentage difference $\left\lvert\frac{\hat{\lambda}_i-\lambda_i}{\lambda_i}\right\rvert \times 100$ (%)
$S_1(\tau)$	1	0.25	1.284	1	0	28.4
$S_2(\tau)$	1	0.15625	1.169	0.5	−0.693	133.8
	2	0.25	1.284	1	0	28.4

$$S_1(\tau) = e^{-\tau} \tag{32}$$

$$S_2(\tau) = 0.5e^{-0.5\tau} + e^{-\tau} \tag{33}$$

α was selected to be 1, thus putting a lower limit of 1 Hz to the sampling frequency and leading to the following distribution functions analogous to (6) for the two signals:

$$x_1(t) = \delta(t) \tag{34}$$

$$x_2(t) = \delta(t + \ln 2) + \delta(t) \tag{35}$$

Nonlinear change of variables was performed by multiplying $S(\tau)$ by $e^{\alpha t}$ ($\alpha = 1$), arriving at (4). The discrete form of (4) was obtained by selecting $\Delta t = 0.25$, $n_{max} = 20$, $n_{min} = -107$ making $N = 128$. Values of ξ, N_0 and γ were experimentally selected to be 0.94, 20 and 0.8 respectively. Figs. 4 and 5 are the graphs of distribution functions for $S_1(t)$ and $S_2(t)$ respectively. Table 1 shows the estimated values of decay rates and their percentage deviation from the expected values. From these results it is obvious that this method is useful in detecting the number of components but performs poorly in accurately estimating the decay rates.

4.1. Effect of N_0

As much as possible the value of N_0 must not be very high. The result of such a selection would be to introduce spurious peaks as shown in Fig. 6 for the signal $S_1(\tau)$ with $N_0 = 100$. From experimentation with different values of N_0 we found that the best range of N_0 is between 20 and 32.

4.2. Effect of γ

The choice of a suitable value of γ is critical for the performance of the proposed technique. Small values of γ lead to poor separation as shown in Fig. 7 for $S_1(\tau)$ when $\gamma = 0.2$. Large values of γ lead to missing components as shown in Fig. 8 for $S_2(t)$ when $\gamma = 0.9$. The best range of γ was found to be between 0.6 and 0.8.

5. Experimental verification

The proposed algorithm was also used to postprocess real data obtained from two fluorophores inside a spectrofluorometer. The spectrofluorometer used is SPECTRAmax GEMINI XS from Molecular Devices. The analyzed fluorophores were

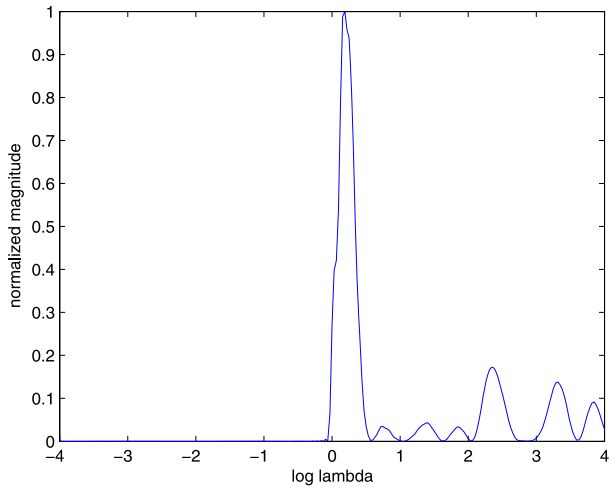

Fig. 6. Effect of large value of N_0.

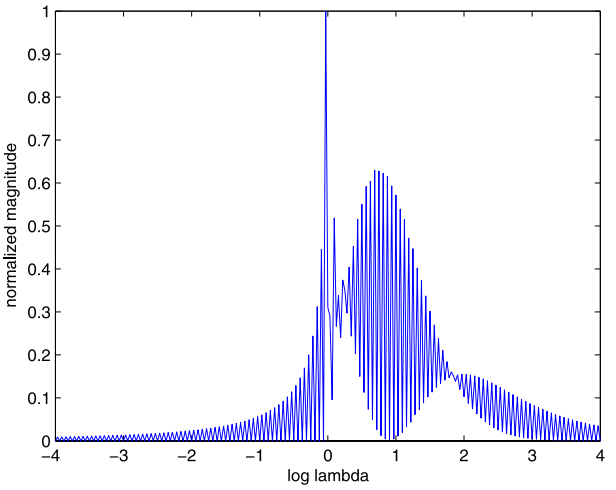

Fig. 7. Effect of small value of γ.

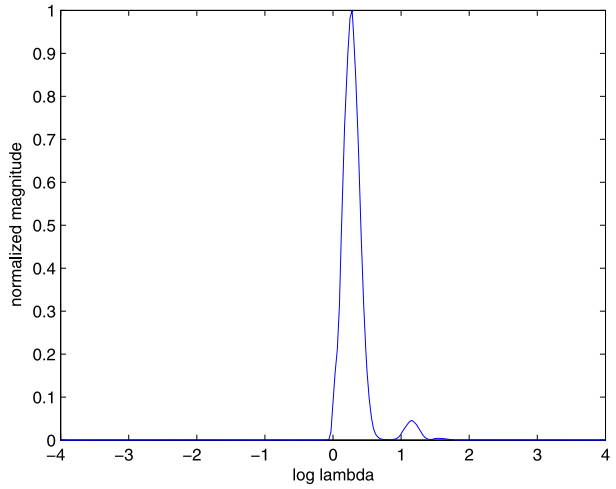

Fig. 8. Effect of large value of γ.

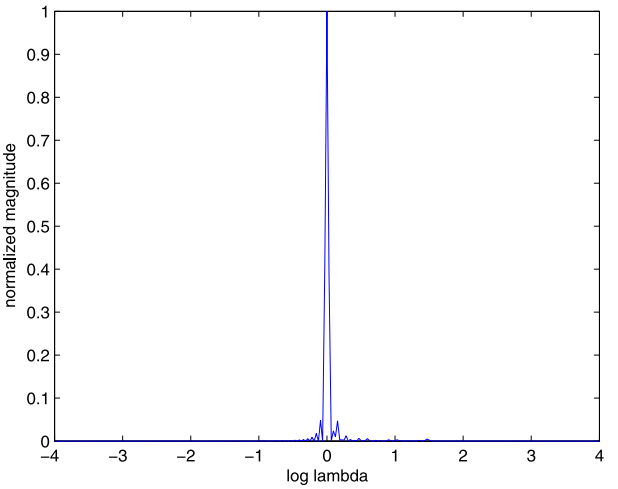

Fig. 9. Graph of distribution function for acridine orange in water.

quinine and acridine orange. The homomorphic deconvolution program was loaded on a PC connected to the spectrofluorometer.

Figs. 9 through 11 show the experimental curves and Table 2 shows the estimated decay rates and their percentage deviation from the expected values. Of course, the results are not better than the simulation results, good in detecting the number of components, but poor in decay rates estimation.

6. Discussion and conclusion

In this paper we have presented the use of cepstral deconvolution to analyze multicomponent exponential signal for two reasons; computational simplicity and in order to avoid the data length constraint and additional modeling associated with inverse filtering. The uncertainty posed by the nonlinearity of the complex cepstrum was avoided by deriving it from the more conveniently computed cepstrum. This was achieved only after the input was converted to minimum-phase by exponential weighting.

However, much as computational simplicity and data length conformity are achieved, results from both simulation and experimental runs leave a lot to be desired. A possible reason for this is the overlapping of regions of support of the conceptual system response resulting from Gardners' transformation and the input signal. Applying homomorphic deconvolution directly to the signal in Eq. (1) would not help matters either. This is for two reasons. One, the individual components are not related by convolution and secondly, the signals are not orthogonal, which makes direct application of any DFT-based technique like homomorphic deconvolution difficult.

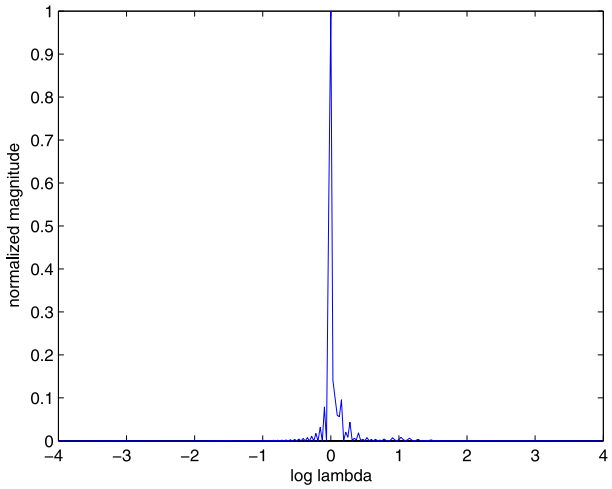

Fig. 10. Graph of distribution function for quinine in water.

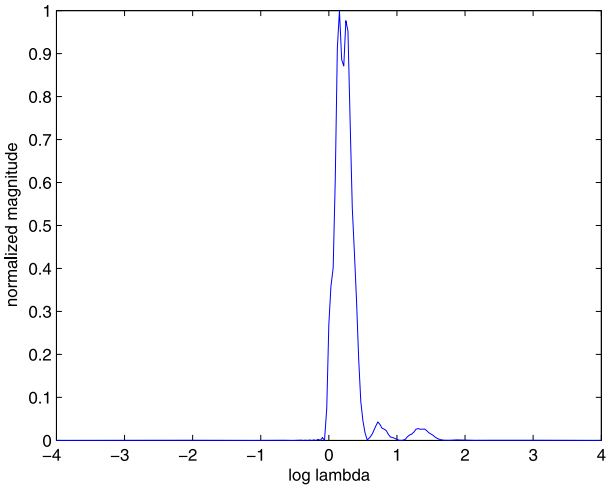

Fig. 11. Graph of distribution function for quinine and acridine orange in water.

Table 2
Percentage differences between the expected and estimated decay rates from experiment.

Fluorophore	i	Estimated log of decay rate ($\ln\hat{\lambda}_i$)	Estimated decay rate ($\hat{\lambda}_i$)	Expected value of decay rate (λ_i)	Expected value of log of decay rate ($\ln\lambda_i$)	Percentage difference $\left\lvert\frac{\hat{\lambda}_i-\lambda_i}{\lambda_i}\right\rvert \times 100$ (%)
Quinine	1	0	1	0.5263	−0.6419	90
Acridine orange	1	0	1	1.8181	0.5978	45
Quinine and acridine orange	Quinine	0.15625	1.169	0.5263	−0.6419	122
	Acridine orange	0.25	1.284	1.8181	0.5978	29.38

Finally, we note that the most crucial step in homomorphic deconvolution is the design of the windowing lifter in the quefrency domain. Homomorphic deconvolution result is highly sensitive to this window since a small error can be exponentially magnified by inappropriate design. With the numerous advantages offered by homomorphic deconvolution, we believe that further research in finetuning this stage is all that is needed to make our approach one of the best, combining computational simplicity, speed, robustness and accuracy in the analysis of multicomponent exponentials.

Acknowledgment

The authors are grateful to the Malaysian Ministry of Higher Education for its grant No. FRGS0207-53.

References

[1] R. Prony, Essai experimentals et analytique, J. Ecole Polytech. Paris 1 (1795) 24–76.
[2] C. Lanczos, Applied Analysis, Prentice Hall, Inc., Englewood Cliffs, NJ, 1956.
[3] D.G. Gardner, J.C. Gardner, G. Lush, W.R. Ware, Method for the analysis of multicomponent exponential decay curves, J. Chem. Phys. 31 (1959) 978–986.
[4] J. Schlesinger, Fit to experimental data with exponential functions using the fast Fourier transform, Nucl. Instrum. Methods 106 (1973) 503–508.
[5] S.T. Nichols, M.R. Smith, M.J.E. Salami, High resolution estimates in multicomponent signal analysis, Tech. Report, Dept. of Electr. Eng., University of Calgary, Alberta, 1983.
[6] M.J.E. Salami, S.N. Sidek, Parameter estimation of multicomponent transient signals using deconvolution and ARMA modeling techniques, J. Mech. Syst. Signal Process. 17 (6) (2003) 1201–1218.
[7] M.J.E. Salami, ARMA models in multicomponent signal analysis, Ph.D. dissertation, Dept. of Electr. Eng., University of Calgary, Calgary, Canada, 1985.
[8] J.E. Sybold, Introduction to RF Propagation, John Wiley and Sons, Inc., New Jersey, 2005.
[9] R.E. Ziemer, W.H. Tranter, Principles of Communications, Systems, Modulation, and Noise, fourth ed., John Wiley and Sons, Inc., Washington, DC, 1995.
[10] A.V. Oppenheim, R.W. Schafer, Discrete-time Signal Processing, Prentice Hall Inc., New Jersey, 1989.
[11] J.M. Tribolet, Seismic Applications of Homomorphic Signal Processing, Prentice Hall Inc., New Jersey, 1979.
[12] A.V. Oppenheim, R.W. Schafer, T.G. Stockham, Nonlinear filtering of multiplied and convolved signals, Proc. IEEE 56 (8) (1968) 1264–1291.
[13] R.W. Schafer, Echo removal by discretized generalized linear filtering, Tech. Rep. 466, M.I.T. Res. Lab. Electron., Cambridge, MA, 1969.